Understanding the mechanisms of electroplasticity from a crystal plasticity perspective

OPEN ACCESS
IOP Publishing
Modelling and Simulation in Materials Science and Engineering
Modelling Simul. Mater. Sci. Eng. **27** (2019) 085006 (28pp) https://doi.org/10.1088/1361-651X/ab43fc

Understanding the mechanisms of electroplasticity from a crystal plasticity perspective

Arka Lahiri[1,3], **Pratheek Shanthraj**[1,2] **and Franz Roters**[1]

[1] Max-Planck-Institut für Eisenforschung GmbH, Max-Planck-Straße 1, D-40237 Düsseldorf, Germany
[2] School of Materials, The University of Manchester, Manchester, M13 9PL, United Kingdom

E-mail: a.lahiri@mpie.de, arkalahiri2009@gmail.com, pratheek.shanthraj@manchester.ac.uk and f.roters@mpie.de

Received 2 July 2019, revised 29 August 2019
Accepted for publication 12 September 2019
Published 30 September 2019

Abstract

Electroplasticity is defined as the reduction in flow stress of a material undergoing deformation on passing an electrical pulse through it. The lowering of flow stress during electrical pulsing has been attributed to a combination of three mechanisms: softening due to Joule-heating of the material, de-pinning of dislocations from paramagnetic obstacles, and the electron-wind force acting on dislocations. However, there is no consensus in literature regarding the relative magnitudes of the reductions in flow stress resulting from each of these mechanisms. In this paper, we extend a dislocation density based crystal plasticity model to incorporate the mechanisms of electroplasticity and perform simulations where a single electrical pulse is applied during compressive deformation of a polycrystalline FCC material with random texture. We analyze the reductions in flow stress to understand the relative importance of the different mechanisms of electroplasticity and delineate their dependencies on the various parameters related to electrical pulsing and dislocation motion. Our study establishes that the reductions in flow stress are largely due to the mechanisms of de-pinning of dislocations from paramagnetic obstacles and Joule-heating, with their relative dominance determined by the specific choice of crystal plasticity parameters corresponding to the particular material of interest.

[3] Author to whom any correspondence should be addressed.

Keywords: electroplasticity, crystal plasticity, constitutive modeling, electrically-assisted manufacturing

(Some figures may appear in colour only in the online journal)

1. Introduction

Electroplasticity (EP) is the phenomenon where a material undergoing deformation displays a drop in flow stress whenever subjected to an electrical pulse. The discovery of this phenomenon can be credited to Troitskii and Likhtman [1] who first observed the reductions in flow stress while passing current pulses through Zn single crystals. Since then it has been recognized that repeated application of the electrical pulses in quick succession during deformation lower the flow stress not only during the pulses but also between the pulses [2–4]. Thus, repeated electropulsing during deformation mimics the attributes of hot working, albeit at a much lower energy cost. This has prompted development of industrial manufacturing paradigms like electrically-assisted manufacturing (EAM) and electroplastic manufacturing processing (EPMP) which leverage the phenomenon of EP on an industrial scale. There are several reviews of EAM, EPMP, and the phenomenon of EP which can serve as useful references in this regard [5–8].

Even as there are increased efforts to harness the benefits of EP in the manufacturing industry, the mechanisms contributing to EP continue to be poorly understood. Researchers over the years have proposed several different theories to explain the reductions in flow stress during electropulsing but without achieving any consensus about the mechanism which dominates the phenomenon of EP. The earliest theory to explain the electroplastic softening is that of Joule-heating; the electrical energy passed to the material is converted to heat, leading to thermal softening of the material. This is the simplest explanation of EP but it is far from being unanimously accepted. Several experiments report the temperature rise due to a single electrical pulse to be too small to be commensurate with the reductions in flow stress [5, 9, 10], while some later studies attribute the observed softening during electropulsing solely to Joule-heating [11, 12]. The ambiguity surrounding Joule heating as the dominant mechanism for EP prompted development of theories which could explain the reductions in flow stress without invoking a rise in temperature of the material. Sprecher *et al* and Conrad *et al* [5, 9], present the first among the athermal theories, which is based on the transfer of momentum from the flowing electrons to the dislocations. It is also known as the 'electron-wind force' theory and was conjectured to be the principal contributor to EP till Molotskii and Fleurov [13] presented an analysis which demonstrated its effect to be small compared to the reductions in flow stress observed during experiments. Molotskii and Fleurov [13, 14] also present a different explanation for the reductions in flow stress. They claim that the induced magnetic field due to the applied current alter the electronic states of the bonds between the obstacles and the dislocation cores which promote de-pinning of dislocations from such obstacles. Their theory requires the obstacles to be paramagnetic in character. The most prominent example of such obstacles are forest dislocations [15], which constitute one of the biggest contributors to flow hardening. Molotskii and Fleurov [13, 14] also present an analysis of the reductions in flow stress due to such an effect and find the softening to be quite substantial compared to the two earlier mechanisms.

To date, the theories of Joule-heating, electron-wind force, and de-pinning from paramagnetic obstacles are the most commonly invoked explanations for instances of EP observed in different materials. The lack of agreement within the scientific community as to which

mechanism dominates the electroplastic behavior is partly because of the difficulty involved in experimentally validating the de-pinning of dislocations and the electron-wind force on dislocations due to electropulsing. There are *in situ* TEM studies where dislocation motion is observed during electropulsing of thin-films [16, 17]. But more recent studies [18, 19] claim that no difference in dislocation activity is observed under current pulsing. It has to be noted that in all these observations there is no concurrent applied strain while electropulsing. Thus, in these studies, the imaged dislocations are static while the current pulses are applied and hence the tests may fail to recognize whether larger segments of dislocations have been freed due to de-pinning. Similarly, the validity of the electron-wind force theory also cannot be ascertained with certainty through such experiments as the transfer of momentum from the electrons to the dislocations may not constitute a high enough force by itself to cause dislocation motion.

With there being no clear understanding of the relative magnitudes of softening induced by different mechanisms of EP through experiments, modeling could play a key role in resolving this issue. There exists several crystal plasticity studies in literature which have tried to model electrically assisted forming [20–24]. In a couple of such studies [21, 24] constitutive models are presented which explain the envelope of the global stress-strain curve during frequent electropulsing without modeling the reductions in flow stress during electropulsing. The global softening of the material is captured phenomenologically without the consideration of any physical mechanisms other than Joule-heating. On the other hand, in [22, 23], the reductions in flow stress during pulsing are also modeled along with the global softening of the material due to repeated electropulsing. These phenomenological crystal plasticity models only allow an empirical consideration of the softening due to Joule-heating and electron-dislocation interactions and do not consider any particular athermal mechanism of softening. As these models do not implement the possible mechanisms of EP explicitly, the questions regarding the relative importance of the proposed mechanisms continue to remain unresolved.

In this paper, our objective is to understand the relative importance of the three theories of EP, namely, thermal softening, electron-wind force, and paramagnetic depinning of dislocations, in producing the reductions in flow stress during electropulsing. In order to achieve this, we employ a dislocation density based crystal plasticity model and extend it to include the different mechanisms proposed for EP. We then perform simulations of uniaxial compression of a representative polycrystalline sample where we pass a single electrical pulse during the loading process and analyze the reduction in flow stress achieved when each of these mechanisms is active. This allows us to develop an understanding of the reductions in flow stress caused by each of these mechanisms and we probe their dependencies on relevant parameters of the crystal plasticity model. A major novelty of our approach from the previous attempts at modeling EP is the fact that we use a dislocation density based crystal plasticity model which provides a physical framework for the introduction of the mechanisms of EP, in contrast to the phenomenological and empirical approaches of earlier studies. This also means that the crystal plasticity parameters employed in our study have a physical significance and can be determined from literature. We utilize this flexibility to select a parameter set for our simulations which is representative of a generic FCC material and hence our conclusions are not limited to any one particular material displaying EP. Our paper is organized in the following manner. First, we present the crystal plasticity model, which is followed by sections which extend the model to include athermal and thermal (Joule-heating) mechanisms of EP. We then present our results, following which we discuss the implications of our study and lay out the possibilities for generalizing the model further to materials belonging to other crystal structures.

2. Crystal plasticity model

We will be using a dislocation density based crystal plasticity model which is described in detail by Wong *et al* [25]. As discussed in the previous section, all the mechanisms of EP are mediated exclusively by dislocation motion. So, in our discussion, we are not going to invoke the other mechanisms which contribute to plasticity, e.g. twinning and transformation induced plasticity (TWIP, TRIP). Our discussion will begin with a review of the kinematic and constitutive relationships of the model.

2.1. Kinematic and constitutive relationships

The imposed deformation gradient $\boldsymbol{F}$ is decomposed into elastic ($\boldsymbol{F_e}$) and plastic ($\boldsymbol{F_p}$) contributions following [26]

$$\boldsymbol{F} = \boldsymbol{F_e}\boldsymbol{F_p}. \tag{1}$$

The stress is computed from the elastic strain by assuming a linear elastic material

$$\boldsymbol{S} = \mathbb{C}(\boldsymbol{F_e}^T\boldsymbol{F_e} - \boldsymbol{I})/2, \tag{2}$$

where, $\boldsymbol{S}$ is the second Piola–Kirchhoff stress tensor and $\mathbb{C}$ is the elastic tensor. The plastic velocity gradient ($\boldsymbol{L_p}$) for a single grain is determined by the stress tensor ($\boldsymbol{S}$) and the variables which define the microstructure ($\boldsymbol{\xi}$) as

$$\boldsymbol{L_p} = \sum_{\alpha=1}^{N_s} \dot{\gamma}^{\alpha}(\boldsymbol{S}, \boldsymbol{\xi})\boldsymbol{m}^{\alpha} \otimes \boldsymbol{n}^{\alpha}, \tag{3}$$

where $\boldsymbol{m}^{\alpha}$ denotes the slip direction and $\boldsymbol{n}^{\alpha}$ denotes the slip plane normal of the slip system α. $\dot{\gamma}^{\alpha}$ denote the shear rates on the individual slip systems denoted by α. N_s denotes the total number of slip systems. The exact form of the dependence of $\dot{\gamma}^{\alpha}$ on $\boldsymbol{S}$ and $\boldsymbol{\xi}$ will be delineated in the next subsection. As discussed earlier, equation (3) considers dislocation motion to be the sole mechanism responsible for plasticity. $\boldsymbol{L_p}$ governs the evolution of the plastic deformation gradient through

$$\dot{\boldsymbol{F}}_{\boldsymbol{p}} = \boldsymbol{L_p}\boldsymbol{F_p}, \tag{4}$$

where $\dot{\boldsymbol{F}}_{\boldsymbol{p}}$ denotes the rate of change of the plastic deformation gradient with time. The equations (1)–(4), can be combined to write

$$\boldsymbol{P}(\boldsymbol{x}) = \boldsymbol{F}\boldsymbol{S} = \boldsymbol{f}(\boldsymbol{x}, \boldsymbol{F}, \boldsymbol{\xi}), \tag{5}$$

where $\boldsymbol{P}$ is the first Piola–Kirchhoff stress tensor determined from $\boldsymbol{S}$. Equation (5) is the crux of the crystal plasticity model and is coupled to the balance of linear momentum through

$$\nabla \cdot \boldsymbol{P} = 0, \tag{6}$$

to simulate a representative volume element (RVE) under static equilibrium. The numerical schemes employed to solve these equations are described in detail elsewhere [27, 28].

2.2. Microstructure (ξ) and shear rates $\dot{\gamma}^{\alpha}$

The microstructure ($\boldsymbol{\xi}$) of the material is described by the mobile edge dislocation density denoted by ρ_m and the immobile dipole dislocation density ρ_d. The motion of the mobile dislocations determines the shear rate $\dot{\gamma}^{\alpha}$ on the slip system α, as given by the Orowan equation

$$\dot{\gamma}^{\alpha} = \rho_m^{\alpha} b_s v_0 \exp\left[-\frac{Q_s}{k_B T}\left\{1 - \left(\frac{\tau_{\text{eff}}^{\alpha}}{\tau_{\text{sol}}}\right)^{p}\right\}^{q}\right]\text{sign}(\tau^{\alpha}), \tag{7}$$

which assumes dislocation glide to be controlled by thermal activation. In equation (7), ρ_m^{α} denotes the mobile dislocation density in the slip system α, Q_s is the activation energy for slip, b_s is the magnitude of the Burgers vector, k_B represents the Boltzmann constant and T is the temperature, τ_{sol} is the stress required to overcome short range obstacles at 0 K, v_0 is the dislocation glide velocity prefactor. $\tau_{\text{eff}}^{\alpha}$ is the effective resolved shear stress written as, $\tau_{\text{eff}}^{\alpha} = |\tau^{\alpha}| - \tau_{\text{pass}}^{\alpha}$, when $|\tau^{\alpha}| > \tau_{\text{pass}}^{\alpha}$, and $\tau_{\text{eff}}^{\alpha} = 0$, otherwise. τ^{α} is the resolved applied shear stress on the slip system α given by $\tau^{\alpha} = \boldsymbol{F}_e^T \boldsymbol{F}_e \boldsymbol{S}(\boldsymbol{m}^{\alpha} \otimes \boldsymbol{n}^{\alpha})$ and $\tau_{\text{pass}}^{\alpha}$ is the passing stress experienced by the mobile dislocations in the slip system α, due to the long range elastic strain fields of the dislocations, defined as

$$\tau_{pass}^{\alpha} = G b_s \left[\sum_{\alpha'=1}^{N_s} \xi_{\alpha\alpha'}(\rho_e^{\alpha'} + \rho_d^{\alpha'})\right]^{1/2}, \tag{8}$$

where G is the shear modulus, and $\xi_{\alpha\alpha'}$ is the interaction matrix of the slip systems. It is important to note that the first instance when $|\tau^{\alpha}|$ is greater than τ_{pass}^{α} defines yielding on the slip system α, where the corresponding value of τ_{pass}^{α} is the slip system level yield stress. $\rho_m^{\alpha'}$ and $\rho_d^{\alpha'}$ are the mobile edge and immobile dipole dislocation densities, respectively, whose evolutions are governed by

$$\dot{\rho}_m^{\alpha} = \frac{|\dot{\gamma}^{\alpha}|}{b_s \Lambda_s^{\alpha}} - \frac{2\hat{d}^{\alpha}}{b_s}\rho_m^{\alpha}|\dot{\gamma}^{\alpha}| - \frac{2\check{d}^{\alpha}}{b_s}\rho_m^{\alpha}|\dot{\gamma}^{\alpha}|, \tag{9}$$

and

$$\dot{\rho}_d^{\alpha} = \frac{2\hat{d}^{\alpha}}{b_s}\rho_m^{\alpha}|\dot{\gamma}^{\alpha}| - \frac{2\check{d}^{\alpha}}{b_s}\rho_d^{\alpha}|\dot{\gamma}^{\alpha}| - \rho_d^{\alpha}\frac{4v_{\text{climb}}}{\hat{d}^{\alpha} - \check{d}^{\alpha}}, \tag{10}$$

respectively. Λ_s^{α} is the mean free path of dislocations. The maximum separation of the glide planes that allow dislocations gliding on them to form dipoles is $\hat{d}^{\alpha}$ while two edge dislocations would get annihilated whenever they are any closer to each other than $\check{d}^{\alpha}$. These distances are calculated to be

$$\hat{d}^{\alpha} = \frac{3Gb_s}{16\pi|\tau^{\alpha}|}, \tag{11}$$

and

$$\check{d}^{\alpha} = C_{\text{anni}} b_s, \tag{12}$$

where C_{anni} is a fitting parameter. The dislocation climb velocity v_{climb} is given by

$$v_{\text{climb}} = \frac{3GD_0\Omega}{2\pi k_B T}\frac{1}{(\hat{d}^{\alpha} + \check{d}^{\alpha})}\exp\left(-\frac{Q_c}{k_B T}\right), \tag{13}$$

where D_0 is the self diffusion coefficient of the material in question, Ω and Q_c are the activation volume and activation energy for climb, respectively. The mean free path Λ_s^{α} is defined as

$$\frac{1}{\Lambda_s^{\alpha}} = \frac{1}{d} + \frac{1}{\lambda_{\text{slip}}^{\alpha}}, \tag{14}$$

where d is the grain size and $\lambda^{\alpha}_{\text{slip}}$ is the average distance traveled by a dislocation before it is stopped by forest dislocations, written as

$$\frac{1}{\lambda^{\alpha}_{\text{slip}}} = \frac{1}{i_{\text{slip}}}\left[\sum_{\alpha'=1}^{N_s} \xi_{\alpha\alpha'}(\rho_m^{\alpha'} + \rho_d^{\alpha'})\right]^{1/2}, \tag{15}$$

where i_{slip} is a fitting parameter which indicates the number of forest dislocations a mobile dislocation is able to overcome before being completely trapped and rendered immobile.

3. Athermal mechanisms of EP

In this section we discuss the major theories explaining EP which do not rely on thermal softening of the material due to Joule heating. We begin with a discussion of the theories by Molotskii *et al* which involve de-pinning of dislocations from obstacles during electropulsing. We follow that up with a review of the theory of electron-wind force assisted dislocation glide as put forth by Conrad *et al*. While considering each of these mechanisms we will also lay out the extensions to the crystal plasticity model required to implement them and attempt a theoretical analysis of the reductions in flow stress caused by each of them wherever possible.

3.1. Paramagnetic de-pinning of dislocations

Molotskii and Fleurov [13] in their seminal paper suggested that de-pinning of dislocations from paramagnetic obstacles is the dominant softening mechanism during electrical pulsing. They demonstrate that the induced magnetic field due to electrical pulsing alters the electronic states in the obstacles and the dislocation cores. These modified electronic states result in a much lower probability of the dislocations being pinned by such obstacles. Forest dislocations qualify as paramagnetic obstacles [15] and they constitute the largest fraction of short range obstacles encountered by dislocations in FCC materials. Thus, any gain in plasticity due to a change in the pinning behavior of such obstacles is likely to be very significant.

It must be noted that the mechanism of de-pinning of dislocations is not dependent on the sense of the current density vector $\boldsymbol{j}$, but only on its magnitude $j = |\boldsymbol{j}|$. So, in this section, whenever we use 'current density' we mean its magnitude represented by j.

In view of the crystal plasticity model we have described in section 2, reductions in flow stress due to de-pinning of dislocations can manifest through several terms in equation (7). We will refer to them as 'sources' of softening within the purview of the primary mechanism of de-pinning of dislocations from paramagnetic obstacles. We investigate each of the sources in the following sub-sections.

3.1.1. Effect of a change in τ_{sol}. As proposed by Molotskii and Fleurov [13, 14], during the application of an electrical pulse, the pinning of dislocations by short range obstacles are weakened. This implies that the inter-obstacle spacing $l_c(0)$ while no current is passed increases to a new value $l_c(j)$ under pulsing. The inter-obstacle distance (l_c) changes as a function of the imposed current density (j) as [13]

$$l_c(j) = l_c(0)\left(1 + \frac{j^2}{j_0^2}\right), \tag{16}$$

where j_0 is a characteristic current density magnitude which corresponds to the magnitude of current density j at which the EP is typically observed for a particular material.

The change in l_c will affect the parameter τ_{sol} in equation (7). τ_{sol} represents the short range resistance experienced by an average dislocation segment. Following the analysis in [29], a critical quantum of force exerted on the dislocation segment given by $\tau_{\text{sol}} b_s l_c$ balances the resistance from the obstacles $\tau_{\text{elem}} b_s w$, where w is the width of the obstacles and τ_{elem} is the stress required by a dislocation line to overcome an obstacle when in contact with the latter. This clearly establishes that τ_{sol} scales inversely as the separation between the short range obstacles (l_c) under constancy of τ_{elem} and w. In other words

$$\tau_{\text{sol}} \propto \frac{1}{l_c}. \tag{17}$$

Combining equations (16) and (17) we can write τ_{sol} as a function of j as

$$\tau_{\text{sol}}(j) = \frac{\tau_{\text{sol}}(0)}{\left(1 + \frac{j^2}{j_0^2}\right)}. \tag{18}$$

Under electropulsing the shear rate on any particular slip system α can be written as

$$\dot{\gamma}^{\alpha}(j) = \rho_m^{\alpha} b_s v_0 \exp\left[-\frac{Q_s}{k_{\text{B}}T}\left\{1 - \left(\frac{\tau_{\text{eff}}^{\alpha}(j)}{\tau_{\text{sol}}(j)}\right)^{p}\right\}^{q}\right] \text{sign}(\tau^{\alpha}). \tag{19}$$

The lowering of τ_{sol} represents lowering of the short range obstacle strength. Thus, under pulsing, similar shear rates ($\dot{\gamma}^{\alpha}$) can be maintained by smaller effective resolved shear stresses $\tau_{\text{eff}}^{\alpha}$ and consequently by τ^{α} which explain the reductions in flow stress on the level of individual slip systems. So, the dependence of τ_{sol} on j (equation (18)), leads to $\tau_{\text{eff}}^{\alpha}$ being a function of j in equation (19).

Molotskii and Fleurov [13] also perform an analysis of the estimated stress drop due to such a softening mechanism. While our formulation of the electroplastic phenomena is on the slip system level, the analysis performed in [13] is for the bulk polycrystalline sample. In order to replicate a similar analysis employing our formulation, we relate the plastic behavior of the bulk sample to that of a single grain employing the concept of Taylor factor (M)

$$\dot{\epsilon}(0) = \frac{1}{M}\sum_{\alpha=1}^{N_s} \dot{\gamma}^{\alpha}(0) = \frac{1}{M}\sum_{\alpha=1}^{N_s}\left(\rho_m^{\alpha} b_s v_0 \exp\left[-\frac{Q_s}{k_{\text{B}}T}\left\{1 - \left(\frac{(\sigma_{\text{eff}}(0)/M)}{\tau_{\text{sol}}(0)}\right)^{p}\right\}^{q}\right]\right)\text{sign}(\tau^{\alpha}), \tag{20}$$

where α runs over all the slip systems in single grain. In equation (20) $\dot{\epsilon}$ is the imposed bulk strain rate and remains constant regardless of whether the system is pulsed or not and σ_{eff} is the effective normal stress along the loading direction and can be thought of as the difference between the applied stress (σ_{appl}) and the long-range resistance (σ_{pass}) which are related to the corresponding quantities τ^{α} and $\tau_{\text{pass}}^{\alpha}$, respectively, for a single slip system. Equation (20), can be modified for an electropulsed sample in the following manner as

$$\dot{\epsilon}(j) = \frac{1}{M}\sum_{\alpha} \dot{\gamma}^{\alpha}(j) = \frac{1}{M}\sum_{\alpha}\left(\rho_m^{\alpha} b_s v_0 \exp\left[-\frac{Q_s}{k_{\text{B}}T}\left\{1 - \left(\frac{(\sigma_{\text{eff}}(j)/M)}{\tau_{\text{sol}}(j)}\right)^{p}\right\}^{q}\right]\right)\text{sign}(\tau^{\alpha}). \tag{21}$$

We divide equation (21) by (20) and impose $\dot{\epsilon}(j) = \dot{\epsilon}(0)$, to write

$$\sum_{\alpha} \rho_m^{\alpha} \exp\left[-\frac{Q_s}{k_B T}\left\{1 - \left(\frac{(\sigma_{\text{eff}}(0)/M)}{\tau_{\text{sol}}(0)}\right)^p\right\}^q\right] \text{sign}(\tau^{\alpha}) = \sum_{\alpha} \rho_m^{\alpha} \exp\left[-\frac{Q_s}{k_B T}\left\{1 - \left(\frac{(\sigma_{\text{eff}}(j)/M)}{\tau_{\text{sol}}(j)}\right)^p\right\}^q\right] \text{sign}(\tau^{\alpha}). \tag{22}$$

Noting that the arguments to the exponentials are not functions of α, we can simplify equation (22) to get

$$\frac{\sigma_{\text{eff}}(0)}{\tau_{\text{sol}}(0)} = \frac{\sigma_{\text{eff}}(j)}{\tau_{\text{sol}}(j)}, \tag{23}$$

and using equation (18) this can be written as

$$\Delta\sigma_{\text{eff}} = \sigma_{\text{eff}}(0) - \sigma_{\text{eff}}(j) = \sigma_{\text{eff}}(0)\frac{j^2}{j_0^2 + j^2}. \tag{24}$$

$\Delta\sigma_{\text{eff}}$ is the difference in effective stresses recorded before and after electropulsing and we can relate it to the applied stress (σ_{appl}) by assuming the averaged long range elastic stress fields to remain constant (σ_{pass}) when τ_{sol} is modified due to electropulsing. So, in terms of the applied stresses

$$\Delta\sigma_{\text{appl}} = \Delta\sigma_{\text{eff}} = \sigma_{\text{eff}}(0)\frac{j^2}{j_0^2 + j^2}. \tag{25}$$

The above equation reveals interesting trends for very low and high values of j. For $j \ll j_0$

$$\Delta\sigma_{\text{appl}} \approx \sigma_{\text{eff}}(0)\frac{j^2}{j_0^2}, \tag{26}$$

which reveals a parabolic dependence on j. When $j \gg j_0$, we get

$$\Delta\sigma_{\text{appl}} \approx \sigma_{\text{eff}}(0), \tag{27}$$

and so the stress drop saturates. The variation of $\Delta\sigma_{\text{appl}}$ as a function of (j/j_0) as predicted by equation (25) has a point of inflection where the curvature $(\partial^2\Delta\sigma_{\text{appl}}/\partial j^2)$ changes from positive to negative and it happens at $(j/j_0) = 1/\sqrt{3} = 0.577$, which marks a transition between the regimes denoted by equations (26) and (27).

It is also important to take note of the assumptions made to arrive at equation (25). The one central assumption of the analysis is that the effective resolved shear stresses $\tau_{\text{eff}}^{\alpha}$ are the same for all the slip systems (α). This assumption allows us to introduce the Taylor factor(M) in equation (20). For crystal plasticity simulations of bulk polycrystalline materials an equality of $\tau_{\text{eff}}^{\alpha}$ for all the slip systems for any particular grain is uncommon and there are considerable differences across the slip systems over all the grains. Also, it has even been observed [30] that the number of active slip systems ($|\tau^{\alpha}| > \tau_{\text{pass}}^{\alpha}$) may vary per grain in a polycrystalline sample and all the grains do not deform similarly as conjectured by Taylor's theory [31]. So, in view of these differences with crystal plasticity implementations, it is reasonable to expect differences between the predictions from simulations and the simplified analysis.

While considering a lowered short-range obstacle strength, Molotskii *et al* ignored other potential ramifications of the de-pinning of dislocations from paramagnetic obstacles. In the

next few subsections, we will explore other possible consequences of dislocation de-pinning within the crystal plasticity framework we have introduced.

3.1.2. Effect of a change in $\lambda^{\alpha}_{\text{slip}}$. Another possible effect of the de-pinning of dislocations is an increase in the distance traveled by the dislocation before being trapped by the forest dislocations ($\lambda^{\alpha}_{\text{slip}}$). Under electropulsing, there is a reduction in the efficacy of forest dislocations which act as short range obstacles to dislocation motion and hence under such a situation a mobile dislocation travels a much larger distance before being rendered immobile. A mobile dislocation overcomes i_{slip} forest dislocations (see equation (15)) before turning immobile and so the average spacing between two forest dislocations determines the total distance traversed by a mobile dislocation ($\lambda^{\alpha}_{\text{slip}}$). As the average distance between two forest dislocations which still pin a mobile dislocation under electropulsing is scaled by the Molotskii factor $(1 + j^2/j_0^2)$, it follows that $\lambda^{\alpha}_{\text{slip}}$ should be scaled by the same factor as well. Hence, we can write from equation (15)

$$\lambda^{\alpha}_{\text{slip}}(j) = \lambda^{\alpha}_{\text{slip}}(0)\left(1 + \frac{j^2}{j_0^2}\right). \tag{28}$$

The effect of change in this length scale on the applied stress is complicated. It alters the evolution of the dislocation densities through equation (9) which in turn can affect the passing stress $\tau^{\alpha}_{\text{pass}}$ as given by equation (8). As $\lambda^{\alpha}_{\text{slip}}$ does not explicitly appear in the Orowan equation an analytical expression relating it to the reductions in flow stress is intractable. However, it is worthwhile to develop an intuitive understanding of the kind of changes prompted in ρ^{α}_{m} and $\tau^{\alpha}_{\text{pass}}$ due to a change in $\lambda^{\alpha}_{\text{slip}}$. From equations (9) and (14) it is clear that ρ^{α}_{m} would increase at a slower rate when $\lambda^{\alpha}_{\text{slip}}$ is larger. Under the assumption that $\dot{\epsilon}(0) = \dot{\epsilon}(j)$, implies $\dot{\gamma}^{\alpha}(0) = \dot{\gamma}^{\alpha}(j)$, a smaller ρ^{α}_{m} necessitates a larger $\tau^{\alpha}_{\text{eff}}$ to maintain a constant $\dot{\gamma}^{\alpha}$. A higher $\tau^{\alpha}_{\text{eff}}$ can be achieved either by lowering of $\tau^{\alpha}_{\text{pass}}$ or by a higher resolved shear stress (τ^{α}). The former can lead to flow softening while the latter can lead to a stress rise during electropulsing and the net change is a combined effect of the two. Thus, there is a possibility of a rise in flow stress instead of a drop due to an increase of $\lambda^{\alpha}_{\text{slip}}$.

3.1.3. Effect of a change in v_0. From the expression of the Orowan equation presented in equation (7), the velocity of dislocations can be expressed as a product of the velocity prefactor v_0 and an Arrhenius term, given as

$$v = v_0 \exp\left[-\frac{Q_s}{k_{\text{B}}T}\left\{1 - \left(\frac{\tau^{\alpha}_{\text{eff}}}{\tau_{\text{sol}}}\right)^{p}\right\}^{q}\right], \tag{29}$$

where

$$v_0 = \nu_G\, d_s, \tag{30}$$

where ν_G is the jump frequency of the dislocations and d_s is the distance moved forward per successful thermal activation event. A typical value of ν_G is $1e11$ s^{-1} [29] and $d_s \approx 1000 b_s$ (see appendix). Granato *et al* [32] suggest that ν_G is independent of the free length of the dislocations between two obstacles and so should remain constant as the odds of pinning by obstacles lower while electropulsing. As an obstacle is overcome by thermal activation, the freed dislocation segment glides until it encounters another obstacle, after which the entire process of thermal activation is repeated. From that argument, d_s is nothing but the inter obstacle spacing(l_c) and hence we have $d_s = l_c$. Thus, under electropulsing, it is reasonable to expect that dislocations would glide larger distances as pinning is less probable. Using the

variation of $l_c(j)$ as given by equation (16) we can write the corresponding scaling relationship for d_s as

$$d_s(j) = d_s(0)\left(1 + \frac{j^2}{j_0^2}\right). \tag{31}$$

Combining equations (30) and (31) we get a scaling relationship for v_0 as given by

$$v_0(j) = v_0(0)\left(1 + \frac{j^2}{j_0^2}\right). \tag{32}$$

An analysis similar to that done for the reductions in flow stress due to τ_{sol} when carried out for this case results in an expression which reads

$$\Delta\sigma_{\text{appl}} = \Delta\sigma_{\text{eff}} = M\tau_{\text{sol}}\left(\frac{k_{\text{B}}T}{Q_s}\right)\log\left(1 + \frac{j^2}{j_0^2}\right), \tag{33}$$

where, we have assumed σ_{pass} to be unaffected by a change in v_0 during pulsing. For situations where $j/j_0 \ll 1$, equation (33) can be approximated as

$$\Delta\sigma_{\text{appl}} = \Delta\sigma_{\text{eff}} = M\tau_{\text{sol}}\left(\frac{k_{\text{B}}T}{Q_s}\right)\frac{j^2}{j_0^2}. \tag{34}$$

3.1.4. Effect of a change in passing stress $\tau^{\alpha}_{\text{pass}}$. Molotskii and Fleurov [33] argue that as the dislocations are de-pinned from short range obstacles, they have a larger free length and hence have a larger geometrical freedom to rotate and re-orient in response to the long range elastic stress fields of other dislocations. Thus, under electropulsing, dislocations can achieve configurations which minimize the strain energy more effectively compared to the situation where no electrical pulses are applied. This implies that larger stresses are needed to force dislocation motion while being pulsed and is an anomaly considering that all other mechanisms induce softening of the material. In the context of the crystal plasticity model described in the paper, $\tau^{\alpha}_{\text{pass}}$ represents the resistance to dislocation motion from the long range strain fields and it should be modified to describe this particular phenomenon. Following the analysis of Molotskii and Fleurov [33] we can modify equation (8) as

$$\tau^{\alpha}_{\text{pass}} = \delta G b_s\left[\sum_{\alpha'=1}^{N_s}\xi_{\alpha\alpha'}(\rho_m^{\alpha'} + \rho_d^{\alpha'})\right]^{1/2}, \tag{35}$$

where, a factor δ is introduced to account for the enhanced elastic interaction. δ is conjectured to have a form given by the following expansion [33]

$$\delta = 1 + \beta\left(\frac{l_c(j) - l_c(0)}{l_c(0)}\right) + \cdots = 1 + \beta\frac{j^2}{j_0^2}, \tag{36}$$

by restricting consideration to the first order terms only. In equation (36) β is a constant determined by fitting and we have made use of equation (16) to arrive at the final form.

We can derive an expression for reductions in flow stress (or increases in flow stress in this case) $\Delta\sigma_{\text{appl}}$ corresponding to the enhanced work hardening due to electropulsing. Following the approach undertaken to derive equation (23), a corresponding relationship for

this case is written as

$$\sigma_{\text{eff}}(j) = \sigma_{\text{eff}}(0), \tag{37}$$

which leads to

$$\Delta\sigma_{\text{appl}} = \Delta\sigma_{\text{pass}} = -\sigma_{\text{pass}}(0)\beta\frac{j^2}{j_0^2}, \tag{38}$$

where we have assumed $M\tau^{\alpha}_{\text{pass}} = \sigma_{\text{pass}}$, M being the Taylor factor. The negative sign in the rhs of equation (38) confirms that the applied stresses would need to be increased when such an effect is operative.

It is important that to note β can be determined by fitting equation (35) to the variation of yield stresses in the material as a function of the imposed current density j [33]. The yield stress of the material corresponds to the value of σ_{pass} when σ_{appl} overcomes σ_{pass} for the first time. Such a quantity is not modified by any other softening mechanism operative due to de-pinning of dislocations and hence is suitable for determining β.

We have considered all possible manifestations of the phenomenon of de-pinning of dislocations during electropulsing. Also, we have presented extensions to the crystal plasticity model which will allow us to simulate the effects of these mechanisms in the later sections. We will discuss the theory of electron-wind force assisted dislocation motion next.

3.2. Electron-wind force: Conrad et al

Conrad *et al* [9] proposed a theory where the electrons drifting under the application of an electric field exert a force on the dislocations. This is known as the 'electron-wind' force and its expression derived by considering the scatter of electrons by dislocations can be stated as

$$\boldsymbol{F_{ew}} = \frac{\rho_D}{N_D} e n_e \boldsymbol{j}, \tag{39}$$

where e is the electronic charge, n_e is the density of free electrons, $\boldsymbol{j}$ is the current density and $\boldsymbol{F_{ew}}$ is the force per unit length of dislocations. In the crystal plasticity model described, plasticity is governed by the motion of the pure edge dislocations which move parallel to themselves along the slip direction $\boldsymbol{m}^{\alpha}$ in the particular slip systems (α). In that case the component of the electron-wind force along the direction of the dislocation motion is given by $\boldsymbol{F_{ew}} \cdot \boldsymbol{m}^{\alpha}$. Assuming an equal fraction of positive and negatively signed dislocations in the material, it is apparent that if the electron-wind force aids the gliding dislocations of one particular sign then it should impede the motion of those belonging to the other sign. This is also pointed out by Molotskii and Fleurov [13] and it implies that the electron-wind force on dislocations is at best a second order effect.

Modeling the effects of the electron-wind force requires an alternate form of the Orowan equation (equation (7)) written as

$$\dot{\gamma}^{\alpha} = \rho_m^{\alpha} b_s v_0 \exp\left[-\left(\frac{Q_s - \tau^{\alpha}_{\text{eff}} V}{k_{\text{B}} T}\right)\right]\text{sign}(\tau^{\alpha}), \tag{40}$$

where the argument of the exponential has been written in an equivalent form assuming the following relationship

$$\Delta G = Q_s - \tau^{\alpha}_{\text{eff}} V^{\alpha} = Q_s\left\{1 - \left(\frac{\tau^{\alpha}_{\text{eff}}}{\tau_{\text{sol}}}\right)^{p}\right\}^{q}, \tag{41}$$

with the Gibbs free-energy of activation denoted by ΔG. The new parameter which appears in the modified Orowan equation (equation (40)) is the activation volume of slip denoted by V^{α}. The new form of the Orowan equation is necessitated to simplify the introduction of the electron-wind force. Following Conrad [9], the effect of the electron-wind force can be modeled as

$$\dot{\gamma}^{\alpha} = \frac{1}{2}\rho_m^{\alpha} b_s v_0 \left\{ \exp\left[-\left(\frac{Q_s - \tau_{\text{eff}}^{\alpha} V^{\alpha} - (\boldsymbol{F_{ew}} \cdot \boldsymbol{m^{\alpha}}) A^{\alpha}}{k_{\text{B}} T} \right) \right] + \exp\left[-\left(\frac{Q_s - \tau_{\text{eff}}^{\alpha} V^{\alpha} + (\boldsymbol{F_{ew}} \cdot \boldsymbol{m^{\alpha}}) A^{\alpha}}{k_{\text{B}} T} \right) \right] \right\} \text{sign}(\tau^{\alpha}), \tag{42}$$

where A^{α} denotes the activation area which is related to the activation volume (V) as, $V^{\alpha} = A^{\alpha} b_s$. Equation (42) treats the electron-wind as an additional force on the dislocations similar to that exerted by $\tau_{\text{eff}}^{\alpha}$. The differential effect of the electron-wind force on dislocations of either sign manifests in equation (42) through opposite signs of the electron-wind force term $(\boldsymbol{F_{ew}} \cdot \boldsymbol{m^{\alpha}})$ for the dislocation densities of either signs $(\rho_m^{\alpha}/2)$. The usefulness of the form of equation (40) is evident here as it allows the electron-wind force to be treated in a manner akin to the effective stress $\tau_{\text{eff}}^{\alpha}$. Equation (42) can be simplified to obtain

$$\dot{\gamma}^{\alpha} = \rho_m^{\alpha} b_s v_0 \exp\left[-\left(\frac{Q_s - \tau_{\text{eff}}^{\alpha}(j) V^{\alpha}}{k_{\text{B}} T} \right) \right] \cosh\left(\frac{(\boldsymbol{F_{ew}} \cdot \boldsymbol{m^{\alpha}}) A^{\alpha}}{k_{\text{B}} T} \right) \text{sign}(\tau^{\alpha}). \tag{43}$$

We are now in a position to revert back to the form of the Orowan equation as given by equation (7) to finally write

$$\dot{\gamma}^{\alpha} = \rho_m^{\alpha} b_s v_0 \exp\left[-\frac{Q_s}{k_{\text{B}} T} \left\{ 1 - \left(\frac{\tau_{\text{eff}}^{\alpha}(j)}{\tau_{\text{sol}}} \right)^{p} \right\}^{q} \right] \cosh\left(\frac{(\boldsymbol{F_{ew}} \cdot \boldsymbol{m^{\alpha}}) A^{\alpha}}{k_{\text{B}} T} \right) \text{sign}(\tau^{\alpha}), \tag{44}$$

which indicates that the electron-wind force introduces the factor, $\cosh(((\boldsymbol{F_{ew}} \cdot \boldsymbol{m^{\alpha}}) A^{\alpha})/(k_{\text{B}} T))$, to the Orowan equation. For a situation where, $((\boldsymbol{F_{ew}} \cdot \boldsymbol{m^{\alpha}}) A^{\alpha}/(k_{\text{B}} T)) \ll 1$, a Taylor-series expansion writes as

$$\cosh\left(\frac{(\boldsymbol{F_{ew}} \cdot \boldsymbol{m^{\alpha}}) A^{\alpha}}{k_{\text{B}} T} \right) = 1 + \frac{1}{2!}\left(\frac{(\boldsymbol{F_{ew}} \cdot \boldsymbol{m^{\alpha}}) A^{\alpha}}{k_{\text{B}} T} \right)^2 + \cdots. \tag{45}$$

So, this indicates that in the event the electron-wind force is small, the factor introduced by it in the Orowan equation is of the second order.

An analytical approach to determine the dependence of reductions in flow stress on the current density (j) is not feasible due to the dependence of the electron-wind force on the direction of dislocation motion on individual slip planes. Such a dependence complicates deriving an analytical expression of the average electron-wind force over the entire bulk sample.

Conrad *et al* [9] also claimed that the activation area A^{α} changes due to electropulsing. The activation area (A^{α}) can be defined as [13]

$$A^{\alpha} = -\frac{1}{b_s}\frac{\partial \Delta G}{\partial \tau_{\text{eff}}^{\alpha}}, \tag{46}$$

and using the last equality of equation (41) in (46), we get

$$A^{\alpha} = \frac{Q_s}{\tau_{\text{sol}} b_s} pq \left\{ 1 - \left(\frac{\tau^{\alpha}_{\text{eff}}}{\tau_{\text{sol}}} \right)^{p} \right\}^{(q-1)} \left(\frac{\tau^{\alpha}_{\text{eff}}}{\tau_{\text{sol}}} \right)^{(p-1)}. \tag{47}$$

From equation (47), it is clear that A^{α} increases under electropulsing as τ_{sol} is scaled down by a factor of $\left(1 + \frac{j^2}{j_0^2}\right)$ following our implementation of Molotskii's theory [13]. So, henceforth in our discussion we do not consider a change in A^{α} explicitly as such an effect is already included in the mechanism of a change in τ_{sol} causing softening.

4. Thermal softening due to Joule-heating

Another source of the reductions in flow stress during electropulsing is conjectured to be the thermal softening of the material due to Joule heating. In order to examine this particular source, we first solve the thermal conduction equation to determine the temperature (T)

$$\rho C_p \dot{T} = \nabla \cdot (\boldsymbol{K} \nabla T) + \dot{Q}, \tag{48}$$

where, $\boldsymbol{K}$ is the thermal conductivity, ρ is the density of the material, C_p is the specific heat capacity, and $\dot{Q}$ is the source term per unit volume. The heat source term is computed as

$$\dot{Q} = \boldsymbol{j} \cdot \boldsymbol{E}, = \boldsymbol{j} \cdot [\boldsymbol{\sigma}_{\boldsymbol{el}}^{-1} \boldsymbol{j}], \tag{49}$$

where $\boldsymbol{j} = \boldsymbol{\sigma}_{\boldsymbol{el}} \boldsymbol{E}$; $\boldsymbol{E}$ is the electric field vector and $\boldsymbol{\sigma}_{\boldsymbol{el}}$ is the electrical conductivity tensor. The evolution of T impacts the shear rates ($\dot{\gamma}^{\alpha}$) as given by

$$\dot{\gamma}^{\alpha} = \rho_m^{\alpha} b_s v_0 \exp\left[-\frac{Q_s}{k_{\text{B}} T(j)} \left\{ 1 - \left(\frac{\tau^{\alpha}_{\text{eff}}(j)}{\tau_{\text{sol}}} \right)^{p} \right\}^{q} \right] \text{sign}(\tau^{\alpha}), \tag{50}$$

where T is now a function of the imposed current density j. An analysis to determine the reductions in flow stress from thermal softening can be carried out in a manner similar to that done for the situation where τ_{sol} changes. In order to do that, we first relate the change in temperature to the imposed current density (j). For a single phase material which is isotropic and homogeneous in all properties, tensors $\boldsymbol{K}$, $\boldsymbol{\sigma}_{\boldsymbol{el}}$ can be reduced to scalars K and σ_{el}. The homogeneity of σ_{el} implies that the source term $\dot{Q}$ is also homogeneous, i.e. every point in the domain experience the same heat source. Under such approximations $\nabla T = 0$ as there is no reason for the T field to be inhomogeneous. This simplifies equation (48) into

$$\rho C_p \dot{T} = \dot{Q}. \tag{51}$$

Solving the above equation yields

$$T(j) = T(0) + Pj^2, \tag{52}$$

where, $P = \Delta t / \sigma_{\text{el}} \rho C_p$ with Δt being the pulse duration. Temperatures at the beginning and at the end of the pulse are denoted by $T(0)$ and $T(j)$. We have ignored cooling of the sample to maintain simplicity of the formulation.

We resume our analysis to determine the dependence of reductions in flow stress on the current density j, and re-tracing the steps employed to derive equation (23) we obtain

$$\left[\frac{1}{T(0)} - \frac{1}{T(j)} \right] = \frac{1}{M \tau_{\text{sol}}} \left(\frac{\sigma_{\text{eff}}(0)}{T(0)} - \frac{\sigma_{\text{eff}}(j)}{T(j)} \right). \tag{53}$$

Now, employing equation (52) in the above equation we get

$$\Delta\sigma_{\text{appl}} = \Delta\sigma_{\text{eff}} = \frac{P}{T(0)} j^2 [M\tau_{\text{sol}} - \sigma_{\text{eff}}(0)], \tag{54}$$

which again assumes constancy of σ_{pass} before and after pulsing. Thus, the reductions in flow stress have a quadratic dependence on the current density j when thermal softening is the operative mechanism. It must be noted that in the presented analysis we have assumed that dislocation climb has not played a role. We will comment on the validity of this assumption based on the temperature rises seen during our simulations of electropulsing.

In the previous sections, we have discussed in detail the crystal plasticity model for simulating EP. We have also provided some analytical expressions relating the stress drop to the current density. At this point we can present the form of the Orowan equation at the slip system level which displays contributions from all the mechanisms of EP

$$\dot{\gamma}^{\alpha}(j) = \rho_m^{\alpha} b_s v_0(j) \exp\left[-\frac{Q_s}{k_B T(j)}\left\{1 - \left(\frac{\tau_{\text{eff}}^{\alpha}(j)}{\tau_{\text{sol}}(j)}\right)^{p}\right\}^{q}\right] \cosh\left(\frac{(\boldsymbol{F_{ew}} \cdot \boldsymbol{m^{\alpha}})A^{\alpha}}{k_B T}\right) \text{sign}(\tau^{\alpha}), \tag{55}$$

where $\tau_{\text{eff}}^{\alpha}(j) = |\tau^{\alpha}(j)| - \tau_{\text{pass}}^{\alpha}$, when $|\tau^{\alpha}(j)| > \tau_{\text{pass}}^{\alpha}$ and $\tau_{\text{eff}}^{\alpha}(j) = 0$, otherwise.

It should be mentioned at this point that we have not considered the skin, pinch, and magnetostriction effects as possible contributors to the phenomenon of EP as their contributions have been established to be small [5, 34] compared to the mechanisms under discussion in this paper. However, thermal expansion due to Joule-heating is recognized to have a bigger contribution compared to skin, pinch and magnetostriction effects [5]. But understandably such an effect is restricted only to tensile tests, and for the compression tests simulated in our paper, thermal expansion can lead to an increase of the flow stress. Thus, due to the lack of generality of the impact of thermal expansion on the flow stress, we have excluded it from our consideration.

In the following section we report simulations of EP through which we attempt to understand the contribution of individual mechanisms to the electroplastic effect.

5. Results

Before presenting the results of our simulations on the electroplastic effect, we would like to discuss a few details about the numerical implementation and the solution technique. We implement the dislocation density based crystal plasticity model in the open-source crystal plasticity software DAMASK [35] and perform RVE simulations of uniaxial compression of polycrystalline samples using the spectral solver [36, 37]. The loads are applied along the x-axis which is completely equivalent to the y and z-axes as the polycrystalline sample in our simulations is chosen to have a random texture. All the simulations are carried out on a $10 \times 10 \times 10$ grid containing 100 grains, each of size 50 μm. The initial dislocation densities are chosen to represent a fully annealed sample and the the mobile dislocation density in each of the 12 slip systems in an FCC material is set to $1e11$ m^{-2} while the initial immobile dipole dislocation density is set to be negligibly small.

Regarding the choice of the crystal plasticity parameters, we must reiterate that our objective is not to simulate the electroplastic effect observed for any particular material, but to explore the characteristics of each of the softening mechanisms of EP. In that regard, we work with typical values of different parameters which are representative of a generic FCC material. We present the values of the parameters related to dislocation glide and climb in table 1,

Table 1. Values of parameters related to dislocation glide and climb.

Parameter	Value
C_{11}	106.75 GPa
C_{12}	60.41 GPa
C_{44}	28.34 GPa
τ_{sol}	7 MPa
d	50 μm
b_s	$2.86e-10$ m
Q_s	$1.6e-019$ J
p, q	1.0
$v0$	$1.0e04$ m s^{-1}
i_{slip}	30.0
C_{anni}	19.0
D_0	$1.76e-05$ m^2 s^{-1}
Q_c	$1.55e-019$ J

Table 2. Values of parameters related to EP.

Parameter	Value
j_0	$3.0e09$ A m^{-2}
β	$1e-03$
(ρ_D/N_D)	$3.3e-025$ Ω m^3
e	$1.6e-019$ C
n_e	$1.8e29$ m^{-3}

Table 3. Values of electrical and mechanical properties.

Parameter	Value
ρ	2700 kg m^{-3}
C_p	900 J kg^{-1} K^{-1}
K	204 W m^{-1} K^{-1}
σ_{el}	$3.5e7$ S m^{-1}

while parameters related to the various mechanisms of EP are mentioned in table 2. The electrical and thermal properties of the material are mentioned in table 3. In experiments of EP, the pulses are usually applied for $\approx$100 μs while their magnitudes range between $1e07 - 1e11$ A m^{-2}. We resort to electrical pulses of similar character in our simulations as well (see caption of figure 1).

Another important point to note is that every parameter in the crystal plasticity model does not equally influence the reductions in flow stress. We will highlight those which have the largest influence, as we discuss each mechanism.

The results presented in this section are in terms of that component of the applied stress tensor which denotes a normal stress along the axis of compression (σ_{appl}). Similarly, the normal component of the imposed strain tensor along the axis of the compression test is referred to as strain (ϵ) in this section.

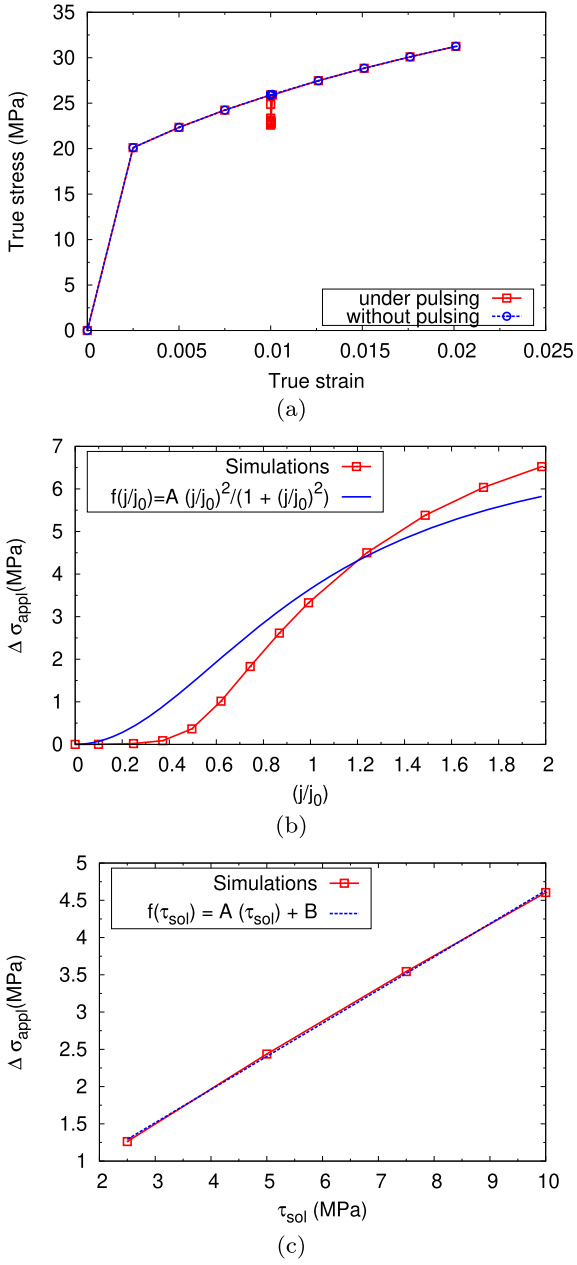

Figure 1. Figures demonstrating different aspects of the reductions in flow stress due to a change in τ_{sol}. (a) Flow curves with and without electropulsing during a compression test. The imposed strain rate is $\dot{\epsilon} = 1e - 03\ \mathrm{s}^{-1}$ and the pulse is applied at a strain of 0.01. The imposed pulse corresponds to $j/j_0 \approx 1$ and is applied for a total time of 60 μs. (b) Reductions in flow stress as a function of (j/j_0). (c) Reductions in flow stress as a function of τ_{sol} at $j = j_0$. The constants A and B in the figure legends are determined by fitting to the simulation data. For (b) and (c) the loading and pulsing details are the same as in (a).

In the discussions that follow, we consider each of the softening mechanisms in isolation. Such an approach should help to delineate the relative contributions of each of the mechanisms towards the electroplastic effect. As there are several possible sources of softening to be considered when de-pinning of dislocations is the operative mechanism, we follow an order which is identical to that used in section 3.1 while discussing them.

We begin with the case where a change in τ_{sol} due to de-pinning of dislocations is the operative mechanism causing flow softening. Referring to the theoretical discussion in section 3.1, we can see that j_0 is a parameter which acts as a normalizing factor to the current density j and hence exerts an influence on the reductions in flow stress obtainable due to dislocation de-pinning. In the absence of a suitable experimental dataset to determine j_0 by fitting, we will choose for its value a quantity which is very similar to that reported for Aluminum [13, 14]. The flow curve presented in figure 1(a) displays a stress drop of around 3 MPa observed coincident with the electrical pulse. The drop is about 12% of the computed flow stress just prior to the point of application of the pulse. The details of the loading and the pulse character are mentioned in the caption of figure 1.

The crystal plasticity extensions to model the softening mechanisms which stem from de-pinning of dislocations involve the ratio (j/j_0) as a crucial parameter. In order to explore the behavior of the reductions in flow stress as a function of the ratio (j/j_0), we record the reductions in flow stress from simulations conducted over a range of values of (j/j_0) and present them in figure 1(b). The curve from simulations display several features of equation (25). These include the parabolic nature of the curve and saturation of the reductions in flow stress at small and high values of (j/j_0), respectively. Thus, it can be claimed that the range of (j/j_0) chosen for our analysis is large enough to capture all the key features of the reductions in flow stress. But even as the softening behavior from simulations qualitatively agrees with the analytical prediction of equation (25), quantitatively there are differences. The deviation of the simulation curve from that due to equation (25) becomes evident when we attempt to fit the simulation data to an expression of the form $f(j/j_0) = A(j/j_0)^2/(1 + (j/j_0)^2)$, with A as the fitting parameter, following equation (25). An important difference between the simulation and the fitted curves is that the point of inflection in the simulation curve no longer manifests at $j/j_0 = 0.577$, but is rather observed at around 0.8. This discrepancy between theory and simulations is not surprising because of two reasons. The first being that of the validity of the scheme which is invoked to derive equation (25) where the behavior of a single grain normalized by a Taylor factor is considered to be representative of the bulk polycrystalline sample. We have already discussed this point in the paragraph following equation (25). The second reason for a possible discrepancy between theory and simulations is due to the assumed constancy of the average long range elastic stress field (σ_{pass}) before and during pulsing, which is used to derive equation (25) from (24). There is no way to verify this assumption as the average long range stress field (σ_{pass}) cannot be explicitly written as a function of τ^{α}_{pass} which prevents it from being determined computationally and can only be related approximately to τ^{α}_{pass} using the Taylor factor (M).

The value of τ_{sol} is expected to have a large bearing on the % drop in stress predicted by equation (25). In order to explore the effect of τ_{sol} further, we focus our attention on the Orowan equation in equation (20) and notice that a particular value of externally imposed $\dot{\epsilon}$ is satisfied by a certain ratio of $(\sigma_{eff}/\tau_{sol})$. Thus, when τ_{sol} changes σ_{eff} should also change to maintain the ratio $(\sigma_{eff}/\tau_{sol})$ constant, implying a direct proportionality between σ_{eff} and τ_{sol}. Using this fact along with a direct proportionality between $\Delta\sigma_{appl}$ and σ_{eff} from equation (25) translates into a similar scaling between $\Delta\sigma_{appl}$ and τ_{sol}. Thus, the reductions in flow stress

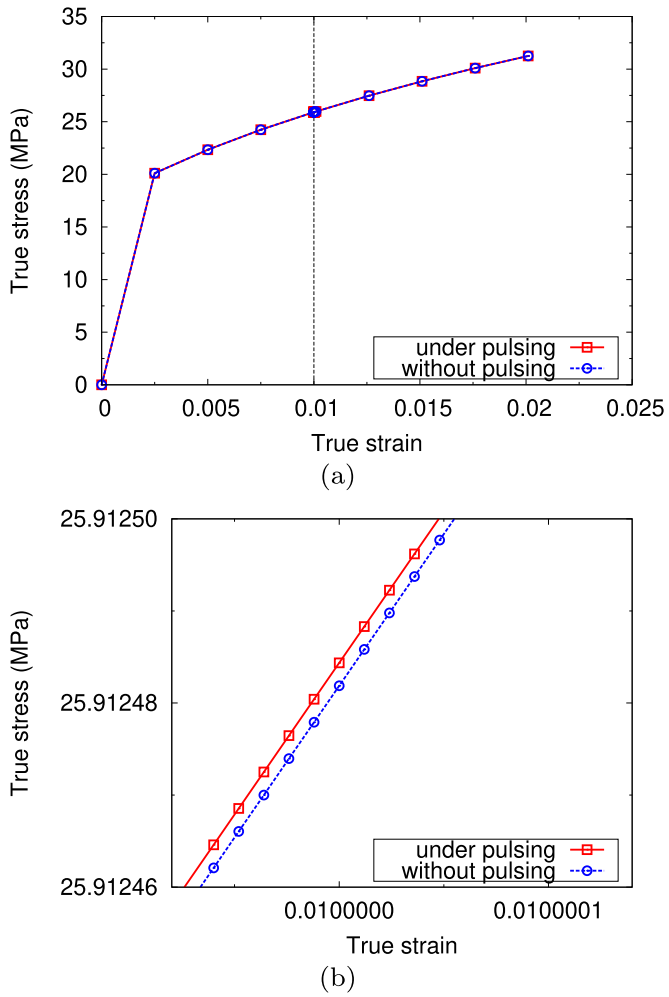

Figure 2. Figures demonstrating the reductions in flow stress due to a change in $\lambda^{\alpha}_{\text{slip}}$. (a) Flow curves with and without electropulsing during a compression test. (b) The magnified version of (a) around a true strain of 0.01. The loading and pulsing details are mentioned in the caption of figure 1.

$\Delta\sigma_{\text{appl}}$ should scale linearly with τ_{sol} and this could indeed be confirmed from figure 1(c) which shows a straight line relationship to exist between $\Delta\sigma_{\text{appl}}$ computed from simulations for different values of τ_{sol} but at a particular value of j. We have also fitted the simulation data with a straight line and found the slope to be 0.44. In view of the importance of τ_{sol} in determining the reductions in flow stress, we present a short discussion in the appendix describing the rational behind the selection of a suitable value for our simulations.

Moving on to the second possible source of reductions in flow stress which is an increase in $\lambda^{\alpha}_{\text{slip}}$, the corresponding flow curve in figure 2(a) hardly shows a difference from the unpulsed one. A slight rise in the flow stress of $\approx 1e-06$ MPa can be discerned when we magnify the flow curves around the strain at which the pulse has been applied as seen in figure 2(b). A rise in flow stress during electropulsing is consistently observed for this particular mechanism across the entire range of (j/j_0) considered in figure 1(b). But as the

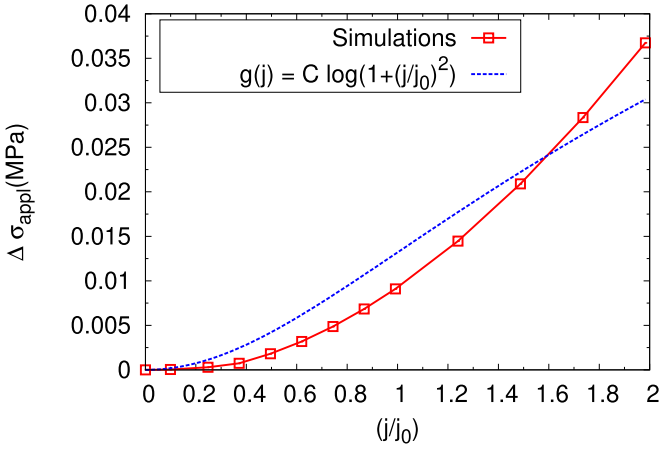

Figure 3. Figure demonstrating the reductions in flow stress due to a change in v_0 as a function of (j/j_0). The loading and pulsing details are mentioned in the caption of figure 1. The constant C is determined by fitting to the simulation data.

increase in stresses are in the same range as the errors due to numerical discretization and precision, a clear trend does not emerge in the variation of $\Delta\sigma_{\text{appl}}$ versus (j/j_0), like observed in figure 1(b). The possibility of an increase of the flow stress instead of a drop when $\lambda^{\alpha}_{\text{slip}}$ increases has been discussed in section 3.1.2.

We now consider the effects of a change in v_0 on the flow curve. A flow curve for this situation is no longer presented as it resembles figure 2(a) and instead we just present a variation of the reductions in flow stress as a function of (j/j_0) in figure 3. It is clear that the reductions in flow stress due to a change in v_0 are about two orders of magnitude lower than those observed for the case where a change in τ_{sol} is the source of softening. Also, the reductions in flow stress appear to be a parabolic function of (j/j_0) and do not display a good fit with an expression of the form predicted by equation (33). The reasons for this deviation are the same as the ones mentioned during the discussion of the reductions in flow stress due to a change in τ_{sol}.

This brings us to the final source of change when dislocations are de-pinned from obstacles, reflected by a change in $\tau^{\alpha}_{\text{pass}}$. The value of the parameter β in equation (38) is chosen to be of the same order of magnitude as that reported in [33](see table 2). As discussed earlier, when de-pinned, larger free length of dislocations respond strongly to the elastic stress fields due to other dislocations which lead to larger strain hardening. Thus, this is a mechanism which always leads to an increase in flow stress during pulsing as confirmed from figure 4 where the reductions in flow stress are presented as functions of (j/j_0). The nature of the curve is parabolic and hence allows a close fit by a function $f(j/j_0) = A(j/j_0)^2$ following equation (38) where A is a fitting constant. The close fit between the form of equation (38) and the simulation data observed in figure 4 is rather fortuitous given the assumptions of the analytical predictions. The maximum value of the rise in $\Delta\sigma_{\text{appl}}$ over the range of current densities considered is insignificant compared to a drop caused by a change in τ_{sol}.

After dealing with the softening sources which are due to the de-pinning of dislocations from obstacles during electropulsing, we now focus on the effects of electron-wind force on dislocations. The variation of the reductions in flow stress due to electron-wind force $\Delta\sigma_{\text{appl}}$ as a function of j has a parabolic character initially but displays a sharper change at higher values of j as evident from the last three points of the curve presented in figure 5. Such a

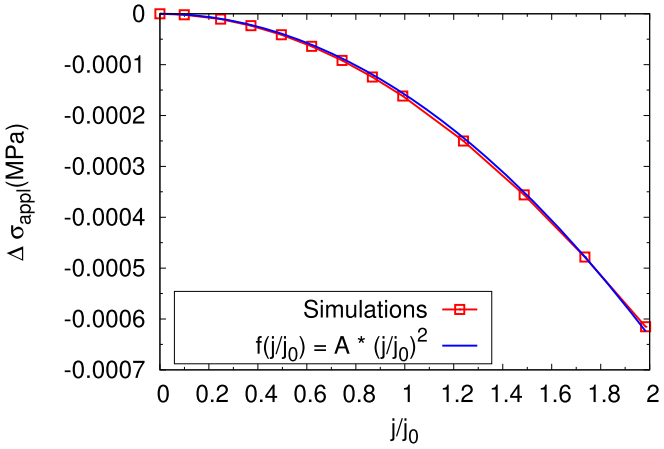

Figure 4. Figure demonstrating the stress rises due to a change in $\tau^{\alpha}_{\text{pass}}$ as a function of (j/j_0). The loading and pulsing details are mentioned in the caption of figure 1.

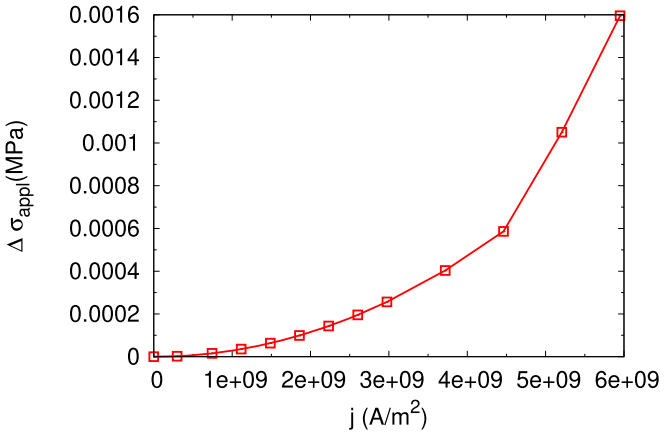

Figure 5. Figure demonstrating the reductions in flow stress due to electron-wind force as a function of j. The loading and pulsing details are mentioned in the caption of figure 1.

behavior correlates well with the nature of the 'cosh' function which is introduced as a factor in equation (44). As claimed by Molotskii and Fleurov [13], we see a very small stress drop of the order of $1e-03$ MPa due to this mechanism. The selection of the relevant parameters like ρ_D/N_D and n_e which control the softening through this particular mechanism is described in the appendix and their values are presented in table 2.

Through the results presented so far, we have developed an understanding of the nature and magnitude of the reductions in flow stress due to the de-pinning of dislocations and the electron-wind force. These mechanisms induce some changes either in the interaction between dislocations and obstacles or modify the forces acting on dislocations. In other words, these mechanisms do not invoke a change in temperature of the material and hence are athermal in character. It is important to determine the quantum of the reduction in flow stress achievable due to Joule heating of the material and compare it against the softening observed

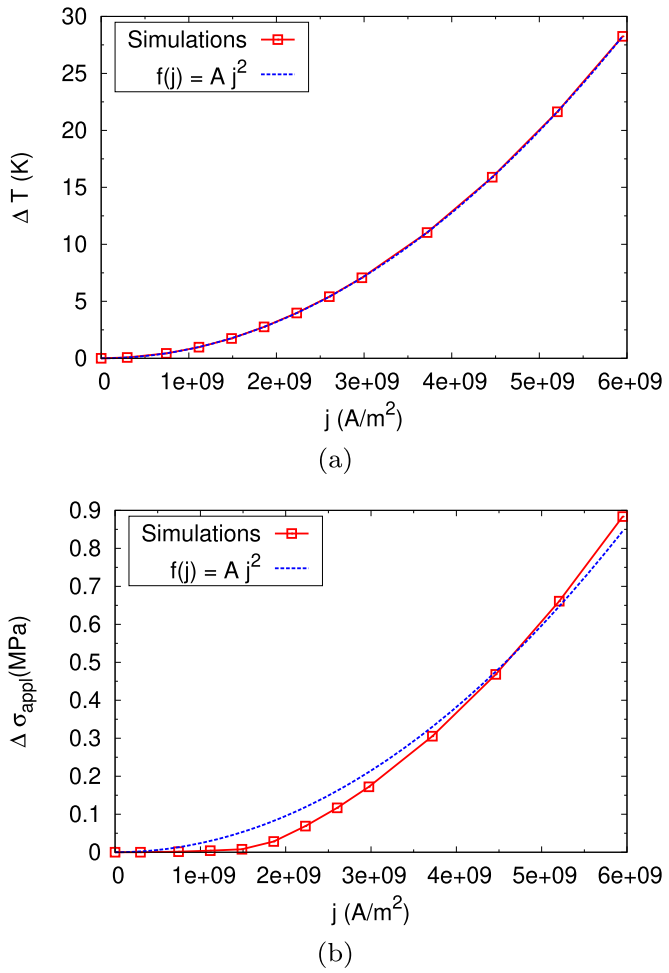

Figure 6. Figures demonstrating the reductions in flow stress due to Joule-heating. (a) Temperature rise as a function of j. (b) Reductions in flow stress as a function of j. The parameter A in the figure legends denote constants which have to be determined by fitting to simulation data. The loading and pulsing details are mentioned in the caption of figure 1.

from athermal means. The first result in this regard is a variation of temperature rise (ΔT) with j as presented in figure 6(a). The corresponding reductions in flow stress are presented in figure 6(b). The variation of temperature rise with j follows a parabolic curve which is in accordance with our analysis expressed by equation (52). The nature of the curve in figure 6(b) is parabolic for $j > 2e09\ \mathrm{A\,m^{-2}}$ and is in accordance with that predicted by equation 6(b). For $j < 2e09\ \mathrm{A\,m^{-2}}$, the softening response seen in simulations is lower than that predicted by our analysis. Such values of j correspond to low temperature rises of $\Delta T < 5\mathrm{K}$, which can be conjectured to be not large enough to cause significant lowering of flow stress due to enhanced thermal activation. In other words, it appears, that unless the temperature exceeds a certain threshold value, there is no significant softening due to Joule-heating. This brings the limitation of analytical expressions like equation 6(b) again to the forefront as the assumptions involved in deriving such expressions are too simplistic

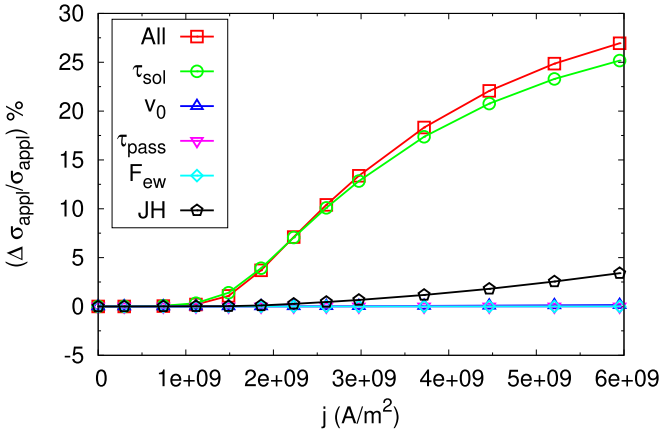

Figure 7. Figure comparing the % reductions in flow stress due to all the mechanisms, plotted as a function of j. In the figure legends, JH denotes Joule-heating, F_{ew} denotes electron-wind force, and 'All' refers to all mechanisms of EP being active. τ_{sol} and v_0 represent reductions in flow stress due to changes in those terms.

compared to actual crystal plasticity simulations. The reductions in flow stress $\Delta\sigma_{appl}$ observed due to Joule-heating are higher than all the other softening sources discussed above except for the case where a change in τ_{sol} causes softening. It can be noted that the activation energies for slip (Q_s) and climb (Q_c) are the key parameters which control the reductions in flow stress due to Joule-heating. We have described the process of selection of Q_s in the appendix, and from figure 6 it is reasonable to argue that the rise in temperature is not enough to cause significant climb of edge dislocations.

We have presented and discussed all the mechanisms and their corresponding sources which result in the electroplastic effect. A graphical summary of our observations is presented in figure 7 where the % drops in stress are plotted as function of the current density j. These figures unambiguously point to modifications in τ_{sol} being the strongest contributor to the reductions in flow stress. Thermal softening due to joule heating is a distant second, while all the other mechanisms produce reductions in flow stress which are at least smaller by an order of magnitude compared to Joule-heating. A curve obtained from a simulation where all the effects are simultaneously active (denoted by a legend 'All' in the figure) lies in close proximity to the τ_{sol} curve and mimics its shape confirming changes in τ_{sol} to be the largest contributor to the reductions in flow stress.

There is a considerable experimental evidence that the magnitudes of the reductions in flow stress are reduced as the the pulses are applied at higher values of strains [5, 10, 14]. In figures 8(a) and (b), we present a variation of the reductions in flow stress due to a change in τ_{sol} and Joule-heating respectively, as functions of the strains at which the sample is pulsed. It can be seen from figure 8(a) that $\Delta\sigma_{appl}$ falls as pulses are applied at higher strains. This could be explained in the following manner. In our crystal plasticity framework, higher strains are microstructurally characterized by a larger value of ρ_m^α (and also ρ_d^α). Invoking the assumption that an imposed $\dot{\epsilon}$ leads to constant values of $\dot{\gamma}^\alpha$ on the different slip planes α, from equation (7) it is clear that for larger values of ρ_m^α at higher strains, smaller values of τ_{eff}^α satisfy equation (7). As σ_{eff} is related to τ_{eff}^α by a Taylor factor, the value of σ_{eff} will also be lowered as the strains increase. The direct proportionality between the reductions in flow stress ($\Delta\sigma_{appl}$) due to a change in τ_{sol} and σ_{eff} due to equation (25) explains the lowered

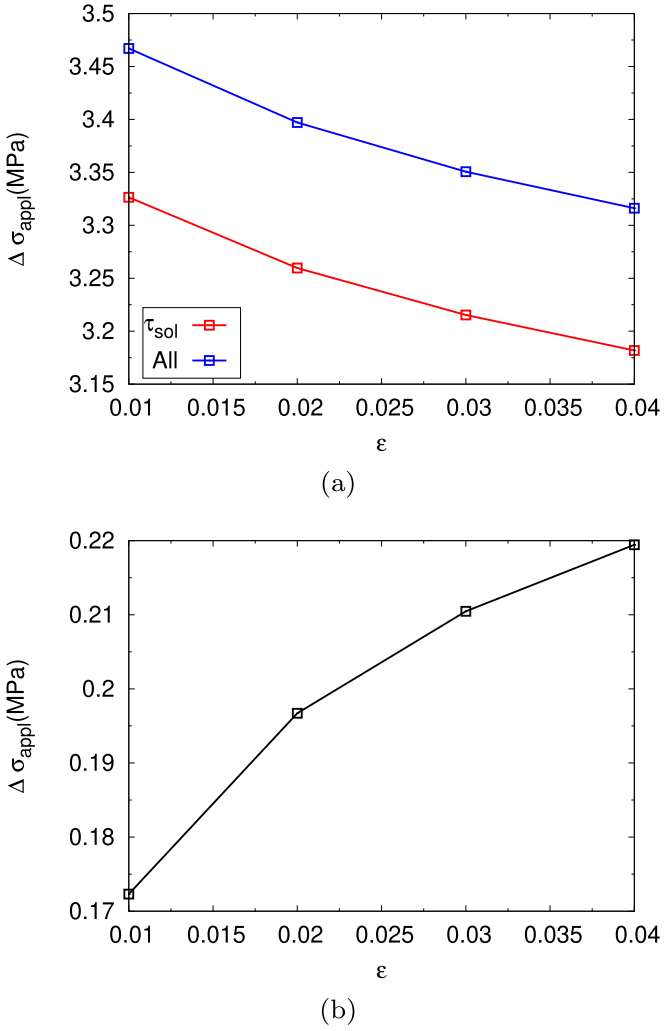

Figure 8. Figures demonstrating the reductions in flow stress ($\Delta\sigma_{\text{appl}}$) due to, (a) a change in τ_{sol} and when all the mechanisms are active, and (b) Joule-heating, with strains (ϵ) at which electrical pulses are applied. The figure legends are explained in the caption of figure 7. Pulses of magnitude $3e09$ A m^{-2} are applied for a total time of 60 μs.

reductions in flow stress ($\Delta\sigma_{\text{appl}}$) at higher values of strains. In other words, at higher levels of strains, plasticity is achieved by generating more mobile dislocations to compensate for the smaller dislocation free paths. Thus, at higher strains, the mechanisms of EP which aid thermal activation of the dislocation segments over short range obstacles can only enhance the much lower dislocation velocity by a smaller factor, compared to that possible at smaller strains.

In contrary to our observations in figure 8(a), the reductions in flow stress due to thermal softening increase with applied strains as shown in figure 8(b). Using the concept of the reduction in σ_{eff} with strain as described in the previous paragraph, the increase in reductions in flow stress observed in figure 8(b) could be immediately explained from equation (54). But

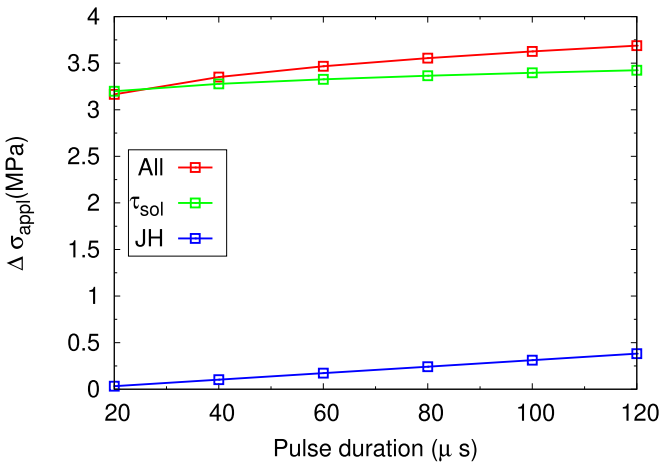

Figure 9. Figure demonstrating the variation of the reductions in flow stress as a function of the pulse width. The current density is maintained at $j = 3e09$ A m^{-2}. The figure legends are explained in the caption of figure 7.

as these changes are an order of magnitude smaller than those observed in figure 8(a), the curve corresponding to the case where all the softening mechanisms are operative, mimics the one representing reductions in flow stress due to a change in τ_{sol} (see figure 8)(a). The influence of the other mechanisms of EP are not considered to be important because they have been seen to produce a negligibly small impact on the reductions in flow stress.

Finally, we probe the effect of pulse duration on the reductions in flow stress as presented in figure 9, where the pulse duration is increased keeping the current density constant. The reductions in flow stress due to a change in τ_{sol} increase gradually as the pulse durations are increased and show signs of saturation at higher pulse durations. This can be explained by discretizing the entire pulse duration into a series of infinitesimal pulses, each lowering the σ_{eff} to a value which becomes the initial σ_{eff} for the subsequent pulse (see equation (24)). Noting that $\sigma_{\text{eff}} \ll \sigma_{\text{appl}}$ and $(\sigma_{\text{eff}}/M) < \tau_{\text{sol}}$, the proportionality of $\Delta\sigma_{\text{appl}}$ with σ_{eff} (see equation (25)) means that the reductions in flow stress increase with the pulse size, but ultimately saturates. Thermal softening due to Joule heating is strongly affected as more electrical energy is introduced into the material as the pulse duration increases. Joule heating being the mechanism which is most sensitive to an increase in pulse duration dominates the overall sensitivity of the electroplastic effect even when all the mechanisms are active as seen in figure 9.

Having reached the end of this section, we will summarize our key observations:

- De-pinning of dislocations produces the largest reductions in flow stress through a change in τ_{sol}.
- Joule-heating is the second largest contributor to the reductions in flow stress but its contribution is still an order of magnitude smaller than that produced by dislocation de-pinning.
- Electron-wind force has negligible contribution to the reductions in flow stress.
- The reductions in flow stress due to de-pinning of dislocations fall as the electrical pulses are applied at higher strains.
- Increasing duration of the electrical pulses increases the reductions in flow stress due to both Joule-heating and dislocation de-pinning.

- As the reductions in flow stress due to de-pinning of dislocations are a strong function of τ_{sol}, it can be expected that for certain combinations of parameters, Joule-heating produces larger reductions in flow stress than that due to de-pinning of dislocations.

In the next section, we discuss a few implications of our results and lay out the possibilities for future work in this direction.

6. Discussion

As already discussed, for the parameter set considered, dislocation de-pinning produces a reduction in flow stress which is an order of magnitude larger than that produced by Joule-heating. But our simulations also demonstrate that it is possible for Joule-heating to supersede the de-pinning of dislocations as the dominant mechanism of EP. This happens when the temperature rise produced in the material is large enough to cause a softening higher than the softening produced by de-pinning of dislocations. In context of this understanding, a few experimental evidences which claim EP to be predominantly a Joule-heating phenomenon can now for the first time be explained consistently within the framework of our model. Examples of such studies are due to Magargee *et al* [12] and Zheng *et al* [38]. It must be noted that the material under consideration in these studies is Ti, which has a hexagonal close packed structure. The fact that there are not enough slip systems in a hexagonal structure to produce a predominantly dislocation mediated plasticity also implies that dislocations interact with forest dislocations much rarely in such materials resulting in smaller values of τ_{sol}, compared to those observed for FCC materials. Hence, it is possible that for such materials, de-pinning of dislocations during electropulsing may not be the dominant softening mechanism. This point has also been raised by Sprecher *et al* [5] where they claim that the interstitial impurities in Ti present the largest barriers to dislocation motion for hexagonal metals. So, for such a material it is quite reasonable that thermal softening due to Joule-heating is the dominant mechanism for EP, especially when the interstitial solutes are not paramagnetic in character. Another work by Goldman *et al* [11] reports no softening in Pb at superconducting temperatures (around 4 K). This could be explained by considering that a change in electronic behavior which induces superconductivity at low temperatures could also potentially inhibit the mechanism of de-pinning of dislocations, which is dependent on electronic states.

With reference to the discussion in the previous paragraph, it can be noted that while the mechanism of de-pinning of dislocations is of central importance to the phenomenon of EP in FCC materials and may be of significance for Hexagonal materials as well, this is not valid for BCC materials, as has already been pointed out by Molotskii [14]. For BCC materials, slip is largely determined by the well known kink-pair mechanism, and the way that mechanism is affected by electropulsing continues to remain unclear. Hence, some experimental suggestions are crucial to formulate an athermal theory of EP for BCC materials. This should lead to a unified crystal plasticity model of EP across all the important classes of materials.

The observation of Gromov *et al* [39] of dislocation motion being controlled by viscous drag during electropulsing instead of being thermally activated is one avenue with interesting possibilities requiring further investigation through experiments. If such a change in the mechanism of dislocation motion is consistently observed for a certain class of materials it should be incorporated in crystal plasticity descriptions of EP like ours, leading to a more nuanced model of EP.

Acknowledgments

The authors gratefully acknowledge the financial support by the DFG Priority Programme SPP 1959/1, 'Manipulation of matter controlled by electric and magnetic field: Toward novel synthesis and processing routes of inorganic materials', Grant Number 319419837.

Data availability

The raw/processed data required to reproduce these findings cannot be shared at this time as the data also forms part of an ongoing study.

Appendix

Here, we present a short description of the process of selection of different parameters which influence the reductions in flow stress during electropulsing. We first describe selection of τ_{sol} which is central to the reductions in flow stress observed due to dislocation de-pinning. The parameters critical to electron-wind force ρ_D/n_d and n_e are discussed next.

A.1. Selection of Q_s and τ_{sol}

The activation energy for slip Q_s is related to the energy of forming a jog as a dislocation intersects a forest dislocation. This energy has been estimated to be between $Gb_s^3/5$ and $Gb_s^3/3$ [40] and we assume it to be

$$Q_s = \frac{1}{4} G b_s^3. \tag{56}$$

For fcc materials, it is often seen that $Gb_s^3 \approx 4$ eV [40], hence $Q_s = 1\ \text{eV} = 1.6e-19$ J from equation (56). When a jog is created by an applied stress τ^* we can write

$$Q_s = \tau^* V, \tag{57}$$

where V is the activation volume defined as

$$V = b_s d_{ac} l_c, \tag{58}$$

with d_{ac} and l_c denote the activation distance and average free dislocation segment length, respectively. For jog formation during forest dislocation interaction, $d_{ac} \approx b_s$ [40], and $l_c \approx 1000 b_s$ [41]. Assuming $b_s = 2.86e-10$ m, using equations (57) and (58), we get, $V \approx 1000 b_s^3$ and $\tau^* \approx 7$ MPa. Conceptually, τ^* is the same as τ_{sol} as the latter represents the stress required for dislocations to overcome short range obstacles like forest dislocations. This exercise allows us to identify two important parameters for our crystal plasticity simulations: $\tau_{\text{sol}} = 7$ MPa and $Q_s = 1.6e-19$ J.

A.2. The parameters influencing the electron-wind force

The two key parameters which affect the electron-wind force are the specific dislocation resistivity ρ_D/N_D and the free electron density n_e. For the former, we use the value stated for aluminum in [42] while we compute n_e using the formula

$$n_e = \frac{f N_{\text{A}} \rho}{M_{\text{A}}}, \tag{59}$$

where, M_A is the atomic mass, f is the number of free electrons per atom, N_A is the Avogadro number and ρ is the density. We compute n_e using the parameters for Aluminum.

ORCID iDs

Arka Lahiri https://orcid.org/0000-0003-2836-2305

References

[1] Troitskii O and Likhtman V 1963 The effect of the anisotropy of electron and γ radiation on the deformation of zinc single crystals in the brittle state *Kokl. Akad. Nauk. SSSR* **148** 332
[2] Roth J T, Loker I, Mauck D, Warner M, Golovashchenko S F and Krause A 2008 Enhanced formability of 5754 aluminum sheet metal using electric pulsing *Transactions of the North American Manufacturing Research Institution of SME* pp 405–12
[3] Salandro W A, Khalifa A and Roth J T 2009 Tensile formability enhancement of magnesium AZ31B-0 alloy using electrical pulsing *37th Annual North American Manufacturing Research Conference, NAMRC 37* 37, pp 387–94
[4] Salandro W A, Jones J J, McNeal T A, Roth J T, Hong S-T and Smith M T 2010 Formability of Al 5xxx sheet metals using pulsed current for various heat treatments *J. Manuf. Sci. Eng.* **132** 051016
[5] Sprecher A, Mannan S and Conrad H 1986 Overview no. 49: on the mechanisms for the electroplastic effect in metals *Acta Metall.* **34** 1145–62
[6] Guan L, Tang G and Chu P K 2010 Recent advances and challenges in electroplastic manufacturing processing of metals *J. Mater. Res.* **25** 1215–24
[7] Nguyen-Tran H-D, Oh H-S, Hong S-T, Han H N, Cao J, Ahn S-H and Chun D-M 2015 A review of electrically-assisted manufacturing *Int. J. Precis. Eng. Manuf.-Green Technol.* **2** 365–76
[8] Ruszkiewicz B J, Grimm T, Ragai I, Mears L and Roth J T 2017 A review of electrically-assisted manufacturing with emphasis on modeling and understanding of the electroplastic effect *J. Manuf. Sci. Eng.* **139** 110801
[9] Conrad H, Sprecher A F, Cao W D and Lu X P 1990 Electroplasticity–the effect of electricity on the mechanical properties of metals *JOM* **42** 28–33
[10] Conrad H 2002 Thermally activated plastic flow of metals and ceramics with an electric field or current *Mater. Sci. Eng.* A **322** 100–7
[11] Goldman P, Motowidlo L and Galligan J 1981 The absence of an electroplastic effect in lead at 4.2 K *Scr. Metall.* **15** 353–6
[12] Magargee J, Morestin F and Cao J 2013 Characterization of flow stress for commercially pure titanium subjected to electrically assisted deformation *J. Eng. Mater. Technol.* **135** 041003
[13] Molotskii M and Fleurov V 1995 Magnetic effects in electroplasticity of metals *Phys. Rev.* B **52** 15829
[14] Molotskii M I 2000 Theoretical basis for electro-and magnetoplasticity *Mater. Sci. Eng.* A **287** 248–58
[15] Molotskii M, Kris R and Fleurov V 1995 Internal friction of dislocations in a magnetic field *Phys. Rev.* B **51** 12531
[16] Livesay B, Donlin N, Garrison A, Harris H and Hubbard J 1992 Dislocation based mechanisms in electromigration *30th Annual Proceedings Reliability Physics 1992, IEEE* pp 217–27
[17] Vdovin E and Kasumov A 1988 Direct observation of electrotransport of dislocations in a metal *Sov. Phys. Solid State* **30** 180–1
[18] Kang W, Beniam I and Qidwai S M 2016 *In situ* electron microscopy studies of electromechanical behavior in metals at the nanoscale using a novel microdevice-based system *Rev. Sci. Instrum.* **87** 095001
[19] Kim S-J, Kim S-D, Yoo D, Lee J, Rhyim Y and Kim D 2016 Evaluation of the athermal effect of electric pulsing on the recovery behavior of magnesium alloy *Metall. Mater. Trans.* A **47** 6368–73
[20] Li D and Yu E 2009 Computation method of metalas flow stress for electroplastic effect *Mater. Sci. Eng.* A **505** 62–4

[21] Roh J-H, Seo J-J, Hong S-T, Kim M-J, Han H N and Roth J T 2014 The mechanical behavior of 5052-H32 aluminum alloys under a pulsed electric current *Int. J. Plast.* **58** 84–99
[22] Hariharan K, Lee M-G, Kim M-J, Han H N, Kim D and Choi S 2015 Decoupling thermal and electrical effect in an electrically assisted uniaxial tensile test using finite element analysis *Metall. Mater. Trans.* A **46** 3043–51
[23] Krishnaswamy H, Kim M J, Hong S-T, Kim D, Song J-H, Lee M-G and Han H N 2017 Electroplastic behaviour in an aluminium alloy and dislocation density based modelling *Mater. Des.* **124** 131–42
[24] Kim M-J, Jeong H-J, Park J-W, Hong S-T and Han H N 2018 Modified Johnson-Cook model incorporated with electroplasticity for uniaxial tension under a pulsed electric current *Met. Mater. Int.* **24** 42–50
[25] Wong S L, Madivala M, Prahl U, Roters F and Raabe D 2016 A crystal plasticity model for twinning-and transformation-induced plasticity *Acta Mater.* **118** 140–51
[26] Lee E H 1969 Elastic-plastic deformation at finite strains *J. Appl. Mech.* **36** 1–6
[27] Diehl M 2016 *High-Resolution Crystal Plasticity Simulations* (Aachen: Apprimus Wissenschaftsverlag)
[28] Shanthraj P, Diehl M, Eisenlohr P, Roters F and Raabe D 2019 Spectral solvers for crystal plasticity and multi-physics simulations *Handbook of Mechanics of Materials* (Singapore: Springer) pp 1–25
[29] Kocks U, Argon A and Ashby M 1975 *Thermodynamics and Kinetics of Slip* (Progress in materials science vol 19) (Oxford: Pergamon)
[30] Peeters B, Seefeldt M, Van Houtte P and Aernoudt E 2001 Taylor ambiguity in BCC polycrystals: a non-problem if substructural anisotropy is considered *Scr. Mater.* **45** 1349–56
[31] Taylor G I 1938 Plastic strain in metals *J. Inst. Met.* **62** 307–24
[32] Granato A, Lücke K, Schlipf J and Teutonico L 1964 Entropy factors for thermally activated unpinning of dislocations *J. Appl. Phys.* **35** 2732–45
[33] Molotskii M and Fleurov V 1996 Work hardening of crystals in a magnetic field *Phil. Mag. Lett.* **73** 11–5
[34] Okazaki K, Kagawa M and Conrad H 1980 An evaluation of the contributions of skin, pinch and heating effects to the electroplastic effect in titatnium *Mater. Sci. Eng.* **45** 109–16
[35] Roters F *et al* 2019 DAMASK-the Düsseldorf advanced material simulation kit for modeling multi-physics crystal plasticity, thermal, and damage phenomena from the single crystal up to the component scale *Comput. Mater. Sci.* **158** 420–78
[36] Eisenlohr P, Diehl M, Lebensohn R A and Roters F 2013 A spectral method solution to crystal elasto-viscoplasticity at finite strains *Int. J. Plast.* **46** 37–53
[37] Shanthraj P, Eisenlohr P, Diehl M and Roters F 2015 Numerically robust spectral methods for crystal plasticity simulations of heterogeneous materials *Int. J. Plast.* **66** 31–45
[38] Zheng Q, Shimizu T, Shiratori T and Yang M 2014 Tensile properties and constitutive model of ultrathin pure titanium foils at elevated temperatures in microforming assisted by resistance heating method *Mater. Des.* **63** 389–97
[39] Gromov V, Gurevich L, Kuznetsov V and Erilova T 1990 Influence of electric current pulses on the mobility and multiplication of dislocations in Zn-monocrystals *Czech. J. Phys.* **40** 895–902
[40] Hull D and Bacon D J 2001 *Introduction to Dislocations* (Oxford: Butterworth-Heinemann)
[41] Evans A and Rawlings R 1969 The thermally activated deformation of crystalline materials *Phys. Status Solidi* b **34** 9–31
[42] Basinski Z, Dugdale J and Howie A 1963 The electrical resistivity of dislocations *Phil. Mag.* **8** 1989–97